Structure of the EF-hand domain of polycystin-2 suggests a mechanism for Ca^{2+}-dependent regulation of polycystin-2 channel activity

Edward T. Petri[a], Andjelka Ćelić[a], Scott D. Kennedy[b], Barbara E. Ehrlich[a], Titus J. Boggon[a,1], and Michael E. Hodsdon[c,1]

[a]Department of Pharmacology, Yale University School of Medicine, 333 Cedar Street, New Haven, CT 06520; [b]University of Rochester School of Medicine, Rochester, NY 14620; and [c]Laboratory Medicine, Yale University School of Medicine, 333 Cedar Street, New Haven, CT 06520.

Edited by Andrew R. Marks, Columbia University College of Physicians and Surgeons, New York, NY, and approved March 26, 2010 (received for review October 27, 2009)

The C-terminal cytoplasmic tail of polycystin-2 (PC2/TRPP2), a Ca^{2+}-permeable channel, is frequently mutated or truncated in autosomal dominant polycystic kidney disease. We have previously shown that this tail consists of three functional regions: an EF-hand domain (PC2-EF, 720–797), a flexible linker (798–827), and an oligomeric coiled coil domain (828–895). We found that PC2-EF binds Ca^{2+} at a single site and undergoes Ca^{2+}-dependent conformational changes, suggesting it is an essential element of Ca^{2+}-sensitive regulation of PC2 activity. Here we describe the NMR structure and dynamics of Ca^{2+}-bound PC2-EF. Human PC2-EF contains a divergent non-Ca^{2+}-binding helix-loop-helix (HLH) motif packed against a canonical Ca^{2+}-binding EF-hand motif. This HLH motif may have evolved from a canonical EF-hand found in invertebrate PC2 homologs. Temperature-dependent steady-state NOE experiments and NMR R_1 and R_2 relaxation rates correlate with increased molecular motion in the EF-hand, possibly due to exchange between apo and Ca^{2+}-bound states, consistent with a role for PC2-EF as a Ca^{2+}-sensitive regulator. Structure-based sequence conservation analysis reveals a conserved hydrophobic surface in the same region, which may mediate Ca^{2+}-dependent protein interactions. We propose that Ca^{2+}-sensing by PC2-EF is responsible for the cooperative nature of PC2 channel activation and inhibition. Based on our results, we present a mechanism of regulation of the Ca^{2+} dependence of PC2 channel activity by PC2-EF.

ion channel | NMR | polycystic kidney disease

Autosomal dominant polycystic kidney disease (ADPKD) is a common life-threatening disorder, characterized by renal cysts (1). Most cases of ADPKD (>95%) are linked with mutations in *Pkd1* and *Pkd2*, which encode polycystin-1 (PC1) and polycystin-2 (PC2); however, the molecular mechanisms underlying ADPKD remain unknown (2). PC1 is a transmembrane protein involved in cell-matrix and/or cell–cell interactions, and PC2 (TRPP2) is a calcium (Ca^{2+}) permeable channel of the transient receptor potential (TRP) family (2). PC1 and PC2 colocalize to cilia, where they may enable a mechano/chemosensory response triggering a rise in intracellular Ca^{2+} (3). PC2 also acts as an intracellular Ca^{2+}-release channel (4) in the endoplasmic reticulum (ER) where it interacts with the inositol-1,4,5 trisphosphate ($InsP_3$) receptor and ryanodine receptor (2). Physiological concentrations of cytoplasmic Ca^{2+} modulate wildtype PC2 channels, but not the ADPKD truncation mutant PC2-L703X (4), suggesting that this functional regulation may be mediated by the PC2 C-terminal tail.

Many aspects of PC2 function are mediated by its C-terminal tail (PC2-C), including assembly with PC1 (5, 6), PC2 homooligomerization (7), interaction with PC2 partners (2), and modulation of the Ca^{2+} dependence of PC2 channel activity (4). Through molecular modeling and biophysical analysis we have shown that PC2-C has three functional regions: an EF-hand (PC2-EF) which undergoes Ca^{2+}-dependent conformational changes, a flexible linker, and an oligomeric coiled coil motif (Fig. 1) (7). Using ROBETTA modeling and isothermal titration calorimetry (ITC) Ca^{2+} titration, we have also found that PC2-EF binds Ca^{2+} at a single site (7). Based on these results, we proposed that PC2-EF is a Ca^{2+} sensor that regulates PC2 activity, and that the coiled coil mediates channel oligomerization. Structure determination of the PC2 coiled coil trimer (833–895) has confirmed part of this model (8), but investigation is required into the structural basis of PC2 regulation by Ca^{2+}.

Several Ca^{2+}-dependent channels contain putative EF-hand domains in their C-terminal tails which modulate channel activity. A potassium-aggravated myotonia associated mutation in the assumed EF-hand in $Na_V1.4$ disrupts fast channel inactivation (9), and bestrophin Cl^- and BK channels have been proposed to contain EF-hands which, when mutated, abolish Ca^{2+} sensitivity (10, 11). In polycystin-2-like-1 (polycystin-L), a protein related to PC2, an EF-hand within the C-terminal tail may attenuate channel overstimulation (12).

Ca^{2+} binding to the C-terminal EF-hand in PC2 has been proposed to mediate the Ca^{2+} dependence of PC2 channel activity (13). PC2 channels are activated at low levels of Ca^{2+}, reaches a maximum with increasing concentrations, and is inactivated at higher levels (14). Although phosphorylation of PC2 at S812 raises the threshold $[Ca^{2+}]$ required for activation, Ca^{2+}-dependence curves for nonphosphorylatable PC2 mutants (S812A) remain bell-shaped (14). Thus, another mechanism must be responsible for conferring Ca^{2+} dependence to PC2. Interestingly, the $[Ca^{2+}]$ required to inhibit S812A PC2 channels (14) is approximately equal to the K_d of Ca^{2+} binding to PC2-C (7), suggesting a critical role for Ca^{2+} binding by the EF-hand within PC2-C.

The EF-hand may be critical for PC2 channel function, and ADPKD mutations N720X, ΔL736-N737, R742X, and Y762X occur within PC2-EF (http://pkdb.mayo.edu). Also, in cultured cells, cytoplasmic Ca^{2+} can be regulated by PC2—an effect abrogated in R742X (4). To describe the role of the EF-hand in Ca^{2+}-dependent regulation of PC2 channels and the structural basis of PC2-EF Ca^{2+} binding, we have determined the NMR structure and dynamics of Ca^{2+}-bound PC2-EF.

Author contributions: E.T.P., A.C., B.E.E., T.J.B., and M.E.H. designed research; E.T.P., A.C., S.D.K., and M.E.H. performed research; M.E.H. contributed new reagents/analytic tools; E.T.P., A.C., S.D.K., B.E.E., T.J.B., and M.E.H. analyzed data; and E.T.P., A.C., B.E.E., T.J.B., and M.E.H. wrote the paper.

The authors declare no conflict of interest.

This article is a PNAS Direct Submission.

Data deposition: NMR, atomic coordinates, chemical shifts, and restraints have been deposited in the Protein Data Bank, www.pdb.org (PDB ID code 2KQ6) and BioMagResBank, www.bmrb.wisc.edu (accession no. 16590).

[1]To whom correspondence may be addressed. E-mail: Titus.Boggon@yale.edu or Michael.Hodsdon@yale.edu.

This article contains supporting information online at www.pnas.org/lookup/suppl/doi:10.1073/pnas.0912295107/-/DCSupplemental.

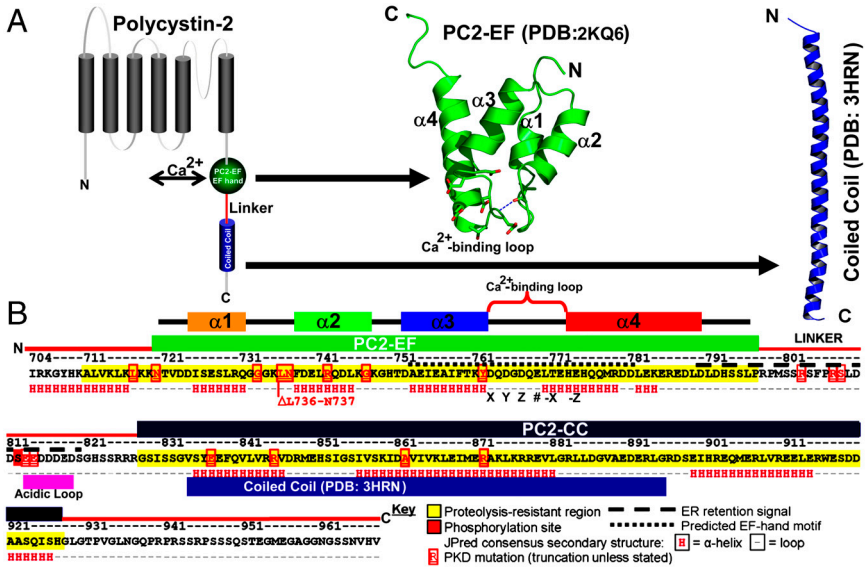

Fig. 1. Molecular architecture of Polycystin-2. (*A*) PC2 contains three functional regions in its C-terminal tail: PC2-EF (green sphere and NMR structure) which undergoes Ca^{2+}-dependent conformational changes, a linker (red), and oligomeric coiled coil (blue cylinder and cartoon crystal structure). (*B*) Sequence of the PC2 C-terminal tail: PC2-EF (green), linker (red), and coiled coil (PC2-CC, blue). Helices α1–4 in PC2-EF are orange, green, blue, and red bars. Residues in the coiled coil X-ray structure are shown as a blue bar (8). Ca^{2+}-binding residues are labeled X, Y, Z, #, -X, and -Z. ADPKD mutations (http://pkdb.mayo.edu) are highlighted (red boxes).

Results

NMR Structure of the C-Terminal EF-Hand Domain of PC2 in the Presence of Ca^{2+}. Chemical shifts (^{1}H, ^{13}C, and ^{15}N) for Ca^{2+}-bound PC2-EF (N720-P797) were assigned for backbone, side chain, and ~90% of ^{1}H resonances. Automated NOESY interpretation was done in CYANA (15), and refinement in Xplor-NIH (16) with automated hydrogen-bond potentials, conformational and residual dipolar coupling (RDC) restraints (*SI Methods*). The final ensemble (Fig. 2) was validated with Protein Structure Validation Software (PSVS) (17) with no violations above tolerance and good packing and geometry (Table 1).

PC2 Contains a Ca^{2+}-Sensitive EF-Hand in its C-Terminal Tail. PC2 is predicted to contain an EF-hand in its C-terminal tail (E754-L782) (5). We isolated a proteolytically stable domain (PC2-EF: N720-P797) and have shown previously that it binds Ca^{2+} noncooperatively at a single site ($K_d \sim 214$ μM) by ITC, and undergoes a Ca^{2+}-dependent transition from a mostly unstructured (27% α-helicity) to a folded state (45% α-helicity) using circular dichroism spectroscopy (7), a property shared with Ca^{2+}-sensor EF-hands (18). The NMR structure reveals that PC2-EF contains a single Ca^{2+}-binding site in an EF-hand motif comprising the helix α3, Ca^{2+}-binding loop, and helix α4 (Fig. 2*C*). An HLH consisting of helices α1 and α2 is paired with this EF-hand as predicted by our ROBETTA model of PC2-EF (7) (Fig. S1). The PC2-EF fold is reminiscent of dimeric EF-hand pairs, and is organized around two antiparallel loops connected by hydrogen-bonding and van der Waals interactions between L736 of the α1–α2 loop and L770 in the α3–α4 Ca^{2+}-binding loop. However, in contrast with canonical EF-hand pairs (which contain two Ca^{2+}-binding loops), the α1–α2 loop (G732-N737) "GGGKLN" does not contain acidic residues necessary for Ca^{2+} coordination (19), and is shorter than the α3–α4 Ca^{2+}-binding loop (D763-E774) "DQDGDQELTEHE." Interestingly, a pathogenic mutation associated with ADPKD, ΔL736-N737, lies within the α1–α2 loop and likely destabilizes the α3–α4 Ca^{2+}-binding loop. Whereas ADPKD truncation mutations N720X, R742X, and Y762X eliminate the EF-hand and coiled coil, ΔL736-N737 should affect only the EF-hand, implying its importance in PC2 function. The structure of PC2-EF suggests that the EF-hand could modulate PC2 channel activity directly through Ca^{2+} binding.

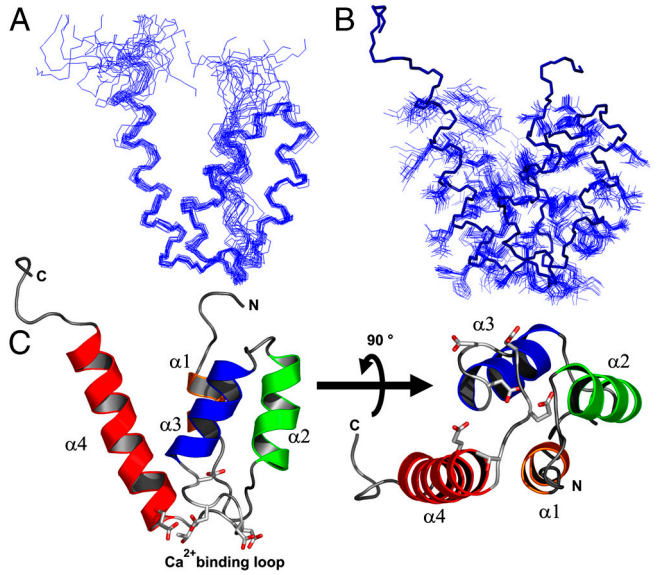

Fig. 2. Structure of Ca^{2+}-bound PC2-EF. (*A*) Backbone ensemble structure of PC2-EF. The top 20 conformers were aligned (backbone rmsd 0.6 Å over I725-D790) (blue ribbons). (*B*) Backbone atoms for the top model (heavy blue ribbon) and side chain atoms for the top 20 conformers (blue lines) *C*) Overall structure of PC2-EF. Helices α1–4 (orange, green, blue, and red), and Ca^{2+}-coordinating residues [Corey-Pauling-Koltun (CPK) sticks] are shown.

Table 1: Overall Structural Statistics

NOE-based distance constraints			506
intraresidue	$i = j$		103
Sequential	$\|i-j\| = 1$		168
Medium	$1 < \|i-j\| < 5$		194
Long	$\|i-j\| \geq 5$		41
Dihedral-angle constraints			148
RDC constraints			59
Distance violations > 0.5 Å			0
rms of distance violation / constraint			0.06 Å
Maximum distance violation			0.44 Å
Dihedral angle violations > 5 °			0
RMS of dihedral angle violation / constraint			1.00°
Maximum dihedral angle violation			4.90°

		Mean Score	SD	Z score
Procheck G factor	(phi / psi only)	0.26	N/A	1.34
	(all dihedral angles)	0.02	N/A	0.12
Prosall		1.07	0.05	1.74
MolProbity clash score		7.91	2.32	0.17
Ramachandran (Procheck)	Most favored	96.7%		
	Additionally allowed	3.3%		

Z scores are with respect to a standard set of ~250 X-ray structures (17).

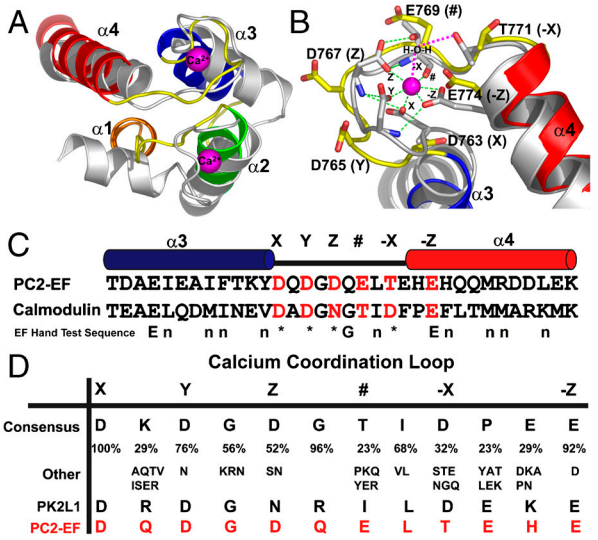

Fig. 3. Comparison of PC2-EF with CaM. (*A*) Structural alignment of PC2-EF (cartoon, helices α1–4 colored orange, green, blue, and red, and loops colored yellow) with Ca^{2+}-bound CaM (PDB ID: 1CLL, white cartoon, magenta Ca^{2+} spheres). (*B*) The PC2-EF Ca^{2+}-binding loop aligned with CaM. CaM Ca^{2+}-coordinating residues are labeled (X, Y, Z, #, -X, -Z, white CPK sticks, magenta Ca^{2+} sphere). Ca^{2+}-coordination bonds are shown as dashes. The residue # coordinates Ca^{2+} with a backbone carbonyl, and -X coordinates Ca^{2+} through an ordered water. Analogous X, Y, Z, #, -X, -Z residues in PC2-EF are shown as yellow CPK sticks. (*C*) Sequence alignment of the EF-hand from PC2-EF and CaM (PC2-EF helices α3 and α4, blue and red). X, Y, Z, #, -X, -Z residues are red and labeled. (*D*) Consensus sequence in EF-hand Ca^{2+}-binding loops (adapted from ref. 19) at X, Y, Z, #, -X, -Z positions. Sequence similarity (%) and common residue substitutions are shown. The Ca^{2+}-binding loop sequence of PC2-EF (red) and polycystin-L (PK2L1, black) is shown.

HLH Motif α1–α2 in PC2-EF Takes the Place of a Ca^{2+}-Binding EF-Hand Motif Found in Paired EF-Hand Domains. In a search of the protein data bank (PDB) for PC2-EF structural homologs, DALI structural alignment (20) identified multiple EF-hand containing proteins: calmodulin (CaM), S100A6, recoverin, and calgranulin (Table S1). The α3–α4 Ca^{2+}-binding loop of PC2-EF superimposes well with these EF-hands, whereas the α1–α2 HLH is structurally divergent (Fig. 3*A* and Fig. S2), and takes the place of the first EF-hand motif found in canonical EF-hand pairs. In Ca^{2+}-bound CaM, α1 is approximately perpendicular to α2, whereas in PC2-EF α1 is nearly parallel with α2.

HLH Motif α1–α2 in PC2-EF May Have Evolved from a Canonical EF-Hand. Sequence and structural features of PC2-EF suggest that the α1–α2 HLH motif may actually be a divergent EF-hand homolog. To investigate this, human PC2-EF (720–797) was aligned using CLUSTALW (21) with PC2 and polycystin-L from vertebrates and invertebrates (Fig. 4*C*). Sequence alignment suggests that polycystin-L channels also contain a divergent HLH motif with only one Ca^{2+}-binding site. However, ancestral invertebrate PC2 contains a canonical dimeric EF-hand with two Ca^{2+}-binding sites (22): the first corresponding to α1–α2 in PC2-EF and the second, α3–α4 (Fig. 5). In contrast, human PC2 has a four-residue deletion in the α1–α2 loop, and substitutions resulting in loss of Ca^{2+}-coordinating residues. The α1–α2 loop still interacts with the Ca^{2+}-binding site of the α3–α4 EF-hand through hydrophobic interactions and hydrogen bonding between L736 and L770, residues conserved in invertebrate PC2 and CaM; thus human PC2-EF has retained some structural features of canonical EF-hand dimers. Sea urchin PC2, which is involved in fertilization, has a different subcellular localization and function than human PC2 (22), and the evolutionary loss of the first Ca^{2+}-binding site may have adapted PC2 for new functions. Structurally, this adaptation would reduce Ca^{2+} affinity

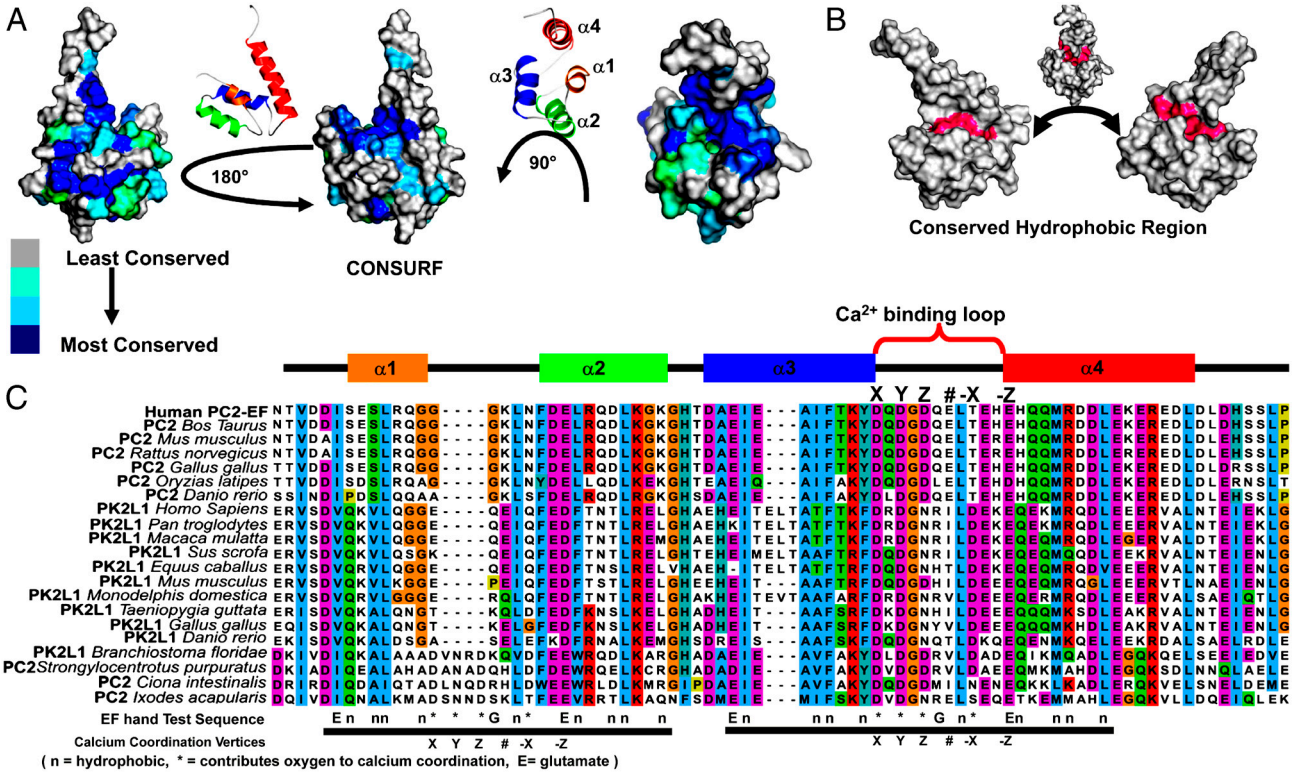

Fig. 4. Sequence conservation and conserved surface analysis of PC2-EF. (*A*) PC2-EF surface conservation (blue = most conserved) from CONSURF. PC2-EF contains a conserved surface in a V-shaped cleft opposite the Ca^{2+}-binding site formed by α1, α3, and α4. (*B*) Hydrophobic saddle in PC2-EF wrapping the conserved surface. (*C*) CLUSTALW alignment of PC2-EF with EF-hands from the C-terminal tails of PC2 and polycystin-L from vertebrates and invertebrates (colored by CLUSTALX conservation). A test sequence corresponding to consensus EF-hands is shown.

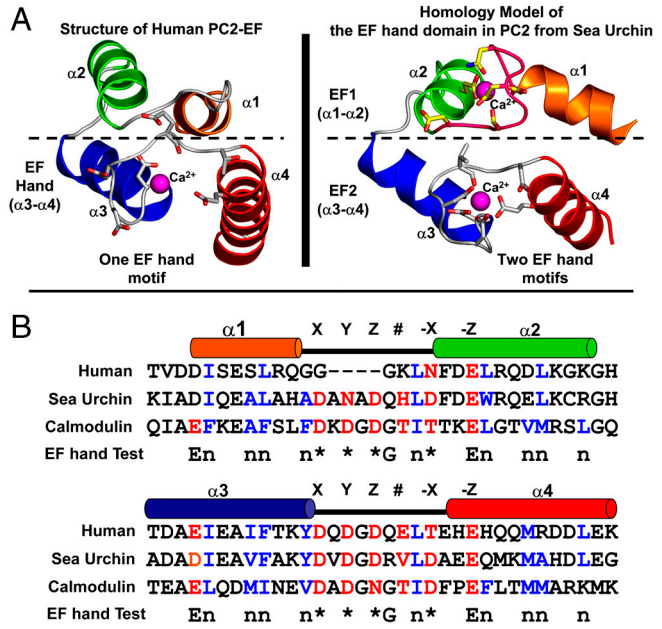

Fig. 5. Comparison of human PC2-EF with a homology model of sea urchin PC2-EF. (*A*) Homology model of sea urchin PC2-EF (*Right*) constructed using Ca^{2+}-bound CaM (PDB ID: 1CLL) as a template in Swiss-Modeller (http://swissmodel.expasy.org/) compared with human PC2-EF (*Left*). Helices corresponding to human PC2-EF α1, α2, α3, and α4 are colored orange, green, blue, and red. Four residues deleted in the α1–α2 loop of human PC2-EF are colored pink in the sea urchin PC2-EF model. Ca^{2+} ions shown (magenta spheres) are from Ca^{2+}-bound CaM. (*B*) Sequence alignment of human and sea urchin PC2-EF with CaM. Helices corresponding to human PC2-EF helices α1 through α4 are colored orange, green, blue, and red. Ca^{2+}-coordinating residues in CaM are labeled X, Y, Z, #, -X, -Z, and colored red. Hydrophobic residues conserved in canonical EF-hands are colored blue. A test sequence corresponding to a consensus EF-hand (18) is shown.

and increase conformational flexibility, enabling Ca^{2+}-sensitive regulation of human PC2.

PC2 Contains a Calmodulin-Like Ca^{2+}-Binding Loop. Ca^{2+} coordination has been defined in crystal structures of Ca^{2+}-bound EF-hands (19). Because Ca^{2+} is not directly observable in our NMR studies, we analyzed our structure and spectra for evidence of Ca^{2+} coordination. Residues predicted to coordinate Ca^{2+} in PC2-EF align well with Ca^{2+}-coordinating residues in CaM (Fig. 3*B*) and rotomer adjustment of side chains would position PC2-EF residues for Ca^{2+} ligation while satisfying NMR restraints [similar variations were reported for S100A6 (23)]. Interestingly, ^{15}N-NOESY peaks corresponding to the hydroxyl proton of T771(-X) and the side-chain carboxyl proton of D767(Z) are visible, consistent with slowed hydrogen exchange due to Ca^{2+} coordination (24). Additionally, linewidths for Ca^{2+}-coordinating residues are increased and have anomalous chemical shifts similar to other EF-hands (25). We have shown previously that Ala substitution at T771 (-X) and E774(-Z) in PC2-EF disrupt Ca^{2+} binding (7) supporting the presence of a Ca^{2+}-binding site in the α3–α4 loop. This Ca^{2+}-binding loop has some deviations from canonical EF-hands, including a Gly to Gln substitution (Q768) (19) (Fig. 3*C*). A similar Gly to Gln substitution exists in S100A6 (23) indicating Gly at this position may not be critical. S100A6 also has micromolar affinity for Ca^{2+} (23) and a Gly to Gln substitution may help reduce Ca^{2+} affinity in PC2-EF to the physiological range for PC2 channel regulation.

PC2-EF Undergoes Conformational Fluctuations in the Ca^{2+}-Bound State. The steady-state $^1H \rightarrow {}^{15}N$ nuclear Overhauser enhancement (ssNOE) for backbone amide ^{15}N nuclei reports fast-timescale (nano- to picosecond) motion. Ordered regions of a protein have ssNOE values >0.8, and decreasing values indicate increased motion (26). Comparison of interresidue NOE restraints (Fig. 6*A*), backbone rmsds and ssNOE values (Fig. 6*B*) to residue number reveals that the α3–α4 EF-hand is structurally dynamic with many ssNOEs <0.5 (Fig. 6*B*). Increased structural fluctuations were measured for the hydrophobic core (I755, I758, Y762, M778, and L782) and Ca^{2+}-binding loop at Q764, D765 (Y) and D767(Z). Similar residues were found to undergo chemical exchange in R_2 and R_1 NMR relaxation experiments (Fig. S3) (27). The high-temperature sensitivity (>50% reduction in ssNOE from 20 to 30 °C) of structural core residues indicates low thermodynamic stability. Interestingly, I755, I758, Y762, M778, and L782 occupy positions which are hydrophobic in CaM and conserved in canonical EF-hands (Fig. 3*B*). Spectral linewidths increase with temperature in this region and the Ca^{2+}-binding loop has increased NMR linewidths, R_2/R_1 ratios and $R_1 * R_2$ products (Fig. S3) (27), which could result from exchange between apo and Ca^{2+}-bound states. In contrast, the motif comprising α2 and the beginning of α3 appears temperature insensitive, and may be a stable core of PC2-EF. In summary, PC2-EF is conformationally dynamic even in the Ca^{2+}-bound state, with structural instability most pronounced in the Ca^{2+}-binding loop and extending into the hydrophobic core, providing a mechanism for PC2 channels to respond to fluctuations in local Ca^{2+} levels. A metastable PC2-EF correlates well with channel flickering and millisecond openings reported for PC2 (4, 14).

PC2-EF May Contain a Conformationally Dynamic Ca^{2+}-Sensitive Protein Interaction Site. Sequence alignment of PC2-EF (Fig. 4*C*) was submitted to CONSURF (28), which predicts functionally important surfaces based on conservation. Conserved residues in PC2-EF form either the hydrophobic core or take part in Ca^{2+} coordination, both important for the PC2-EF fold (Fig. 4

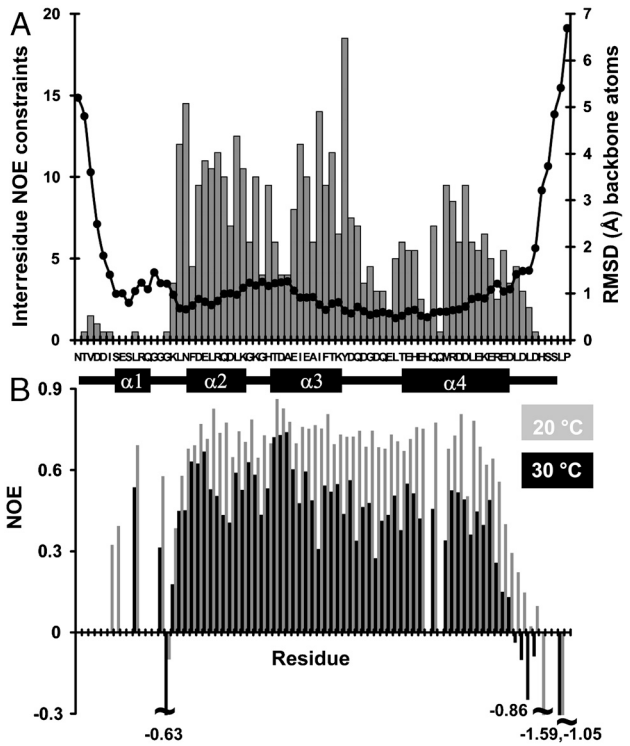

Fig. 6. Interresidue NOE restraints and backbone rmsds compared to steady-state NOE values. (*A*) Number of interresidue NOE constraints (gray bar chart, left axis) per residue overlaid with backbone rmsd per residue calculated as deviation from a mean structure of the top 20 conformers (right axis, scatter plot, black dots). (*B*) Steady-state NOE analysis at 20 °C (gray bars) and 30 °C (black bars) per residue.

A and *C*). CONSURF reveals a conserved hydrophobic "saddle" on the EF-hand in a V-shaped cleft between α3 and α4, suggestive of a protein interaction site (Fig. 4 *A* and *B*). This same region shows significantly increased temperature-dependent mobility (Fig. 6). Given the Ca^{2+}-dependent conformational changes observed in PC2-EF, protein interactions at this site could be Ca^{2+} regulated. Because several proteins interact with PC2 through the C-terminal tail, including polycystin-1 and TRPC1, and these interactions modulate PC2 channel activity (2), it seems plausible that Ca^{2+}-dependent interactions mediated by PC2-EF may be an additional mechanism for PC2 channel regulation.

Cross-Validation of the NMR Structure of PC2-EF Using Residual Dipolar Couplings. We validated our NMR refinement solution by comparing the correlation between experimentally measured RDCs and our structure of PC2-EF using the program PALES (40). Although good agreement [quality factor (Q-factor) 12.1%, R = 99.2%] was found between RDCs predicted by the structure of PC2-EF and experimentally measured Pf1 phage NH (backbone amide) RDCs (Fig. S4*A*), PC2-EF was refined in the presence of these RDCs and positive correlation alone does not confirm structural accuracy. In contrast, the "free" Pearson's R correlation coefficient and "free" Q-factor between withheld experimental RDCs and those predicted for a structure has been proposed as a measure of structural accuracy (29). A random 10% subset of Pf1 phage NH RDCs was withheld from an independent Xplor-NIH refinement for cross-validation purposes and used to calculate the free Q-factor and free Pearson's R-factor (Fig. S4 *E* and *F*) resulting in Q-free = 35.3% and a Pearson's R-free value of 88.0%. Additionally, NH RDCs were measured in an alternate alignment media, 7% strained polyacrylamide gels, to obtain independent alignment tensors for additional cross-validation. These RDCs were not used in refinement. NH RDCs back-calculated from PC2-EF structures refined using Pf1 phage derived RDC constraints correlate well (Q-factor = 29.7%, R = 94.5%) with independent RDCs measured in 7% strained gels (Fig. S4*C*), providing independent validation of our structure. Finally, NH RDCs back-calculated from structures refined while withholding the same random 10% subset of NH RDCs as in Fig. S4*E* correlate with NH RDCs measured in 7% strained gels (Q-overall = 33.3%, R-overall = 92.9%; Fig. S4*F*) resulting in Q-free = 29.5%.

Comparison of PC2-EF with a Previously Reported NMR Structure of the PC2 EF-Hand Domain (PDB: 2KLE). During preparation of this work, another NMR structure of the PC2 EF-hand was published (30) (PDB: 2KLE) with a very different fold from our structure of PC2-EF (Fig. S5). The structure 2KLE appears incompatible with our experimental RDC constraints, and poor correlation was found between 2KLE and NH RDCs measured in Pf1-phage (Q-factor = 97.0%, Pearson's R = 25.0%; Fig. S4*B*) or 7% strained gel (Q-factor = 87.8%, Pearson's R = 43.2%; Fig. S4*D*) (Fig. S4). In light of the differences between 2KLE and PC2-EF, we conducted extensive structure validation tests, and comparisons of these results raise questions about the validity of 2KLE. Using WHATCHECK (31), the PSVS (17), and "Protein Structure Quality Score" (32), we compared PC2-EF and 2KLE in terms of indices of structural validity (Fig. S6). Whereas PC-EF has acceptable *Z* scores (standard deviations from average), 2KLE produced unusually negative *Z* scores between −4.0 and −6.0. *Z* scores < -4.0 are associated with incorrect or improperly refined protein structures (31). In addition, according to the DALI structure comparison server, no structures in the PDB database have folds with significant homology to 2KLE. Finally, the 2KLE fold appears unlikely to support a competent Ca^{2+}-binding site because its EF-hand helices are parallel, restraining the backbone of Ca^{2+}-coordinating residues in opposing directions from the Ca^{2+} ion (Fig. S5 and Fig. S7).

Discussion

In the cell, cytoplasmic concentrations of Ca^{2+} oscillate from subnanomolar to tens of micromolars, with greater concentrations at the ER surface and ciliary plasma membrane (33) where PC2 is localized (34). Ca^{2+} concentrations at the PC2 channel pore may vary widely due to opening of PC2, ryanodine, and $InsP_3$ receptor channels (35). Fluctuations in cytoplasmic Ca^{2+} regulate the activity of wild-type PC2, but not PC2-L703X channels (14), supporting a regulatory role for the C-terminal tail of PC2. We have previously shown that this tail contains an EF-hand which undergoes Ca^{2+}-dependent conformational changes and binds a single Ca^{2+} with micromolar affinity (7). Based on the structure of Ca^{2+}-bound PC2-EF presented here, we propose that Ca^{2+} sensing by PC2-EF modulates PC2 channel activity. We further hypothesize that the α1–α2 HLH motif in PC2-EF has evolved from a canonical EF-hand found in invertebrate PC2 homologs (22) in order to fulfill this regulatory role. The first HLH motif (α1–α2) in PC2-EF evolved a truncated loop, which is unable to bind Ca^{2+} or provide the same stabilizing interactions found in canonical EF-hands. The resulting lowered Ca^{2+} affinity in PC2-EF provides responsiveness to physiologic $[Ca^{2+}]$.

PC2 activity is regulated by Ca^{2+} in a bell-shaped, cooperative manner (14). Cooperativity enables switch-like regulation over a narrow range of ligand concentration (36) and has been reported for Ca^{2+}-regulated channels including the $InsP_3$ receptor (37). Furthermore, the Ca^{2+} dependence of PC2 channel activity displays a Ca^{2+} concentration for inhibition (14) (~10 μM) equivalent to the apparent K_d of Ca^{2+} binding to PC2-C ($K_d \sim 12$ μM) (7), suggesting a link between Ca^{2+} binding and inhibition of channel activity.

We have previously shown by ITC that PC2-EF (720–797) binds Ca^{2+} *noncooperatively* ($K_d \sim 214$ μM) with 1:1 stoichiometry, and that 720–797 with EF-hand motif mutations (T771A/E774A) cannot bind Ca^{2+} (7). Also, 720–797 is monomeric by analytical ultracentrifugation and size exclusion chromatography (7) and does not dimerize upon Ca^{2+} binding even at >1 mM concentration, according to estimates of rotational correlation times (Fig. S3). The lack of cooperative binding is not surprising because 720–797 only contains an EF-hand with a single Ca^{2+} binding site and does not contain a coiled coil domain (7). In contrast, the structure of the PC2 coiled coil domain, 833–895 is trimeric (8) and PC2 704–968 (containing both this coiled coil domain and the EF-hand) does bind Ca^{2+} cooperatively and with ~20-fold higher affinity (7). The proximity of three EF-hands in trimeric PC2 704–968 would be sufficient to enable cooperativity.

We propose a model where Ca^{2+} binding to one EF-hand leads to conformational changes which stabilize the EF-hand from neighboring C-terminal tail(s) in multimeric PC2 channels, which in turn leads to cooperative Ca^{2+} binding and activation of the PC2 channel activity, followed by inhibition upon saturation of available Ca^{2+}-binding sites. ADPKD associated mutations in the C-terminal tail of PC2 would disrupt these functions, contributing to a structural basis for polycystic kidney disease progression.

Methods

See *SI Methods* for further details.

NMR Spectroscopy. PC2-EF (N720-P797) was purified as described (7). NMR samples contained ~1 mM PC2-EF in 2 mM Tris pH 7.4, 150 mM NaCl, 20 mM $CaCl_2$, plus 1 mM PC2-EF, 5% D_2O, 0.05% NaN_3, 10 μM PMSF, leupeptin, and pepstatin. NMR spectra were collected at 30 °C (Varian INOVA 600 MHz) and processed in NMRPipe. Resonance specific chemical shifts were assigned using (2D) ^{1}H-^{15}N HSQC (Heteronuclear Single Quantum Coherence), ^{1}H-^{13}C HSQC, (3D)HNCO, HN(CA)CO, HNCACB, HN(CO)CA, HCACO, HCC(CO)NH, ^{15}N-TOCSYHSQC (Total Correlation Spectroscopy), HCCH-TOCSY,

2D ^{1}H-^{13}C HSQC, and 3D ^{13}C-NOESYHSQC (Nuclear Overhauser Enhancement Spectroscopy) spectra (BioMagResBank accession no. 16590).

Steady-State ^{1}H → ^{15}N NOE Measurements. Steady-state ^{1}H ^{15}N NOE experiments included sensitivity enhancement, water flip-back, and coherence selection via pulse field gradients with 9-s saturation and 6-s recycle delay; 128 transients were collected at 9 kHz (f2) and 2.1 kHz (f1).

R_1 and R_2 NMR Relaxation Rates. T1 and T2 relaxation times were extracted from two series each of ^{1}H-^{15}N HSQC spectra with delays of 100, 300, 500, 700, and 1,000 ms for T1 and 10, 30, 70, 150, 190, and 250 ms for T2, with a 1-s recycle delay. NMR peak heights determined by the "rh" command in SPARKY, and the program CurveFit (38) was used for exponential fitting of R_1 and R_2.

Dihedral Angle and NOE Distance Restraints. Backbone Φ and Ψ torsion (dihedral) restraints were calculated using TALOS. NOESY correlations were identified in 3D ^{15}N-NOESY-HSQC and (aromatic) ^{13}C-NOESY-HSQC in SPARKY and interpreted in CYANA. Seven iterations of automated NOESY interpretation, structure calculation, and restraint analysis yielded final distance restraints. Dihedral angle restraints were included to improve convergence.

Measurement of Residual Dipolar Couplings. Anisotropic orientational restraints were obtained from Ca^{2+}-bound ^{15}N PC2-EF with either 20 mg/mL Pf1 phage, or 7% strained polyacrylamide gel (as described in *SI Methods*), and compared to ^{15}N PC2-EF lacking phage. $^{1}J_{NH}$ coupling constants were measured using a spin-state-selective ^{1}H, ^{15}N-HSQC pulse sequence.

Structure Determination. NOESY interpretations were converted to distance restraints in CYANA, and with dihedral restraints, RDCs, Xplor-NIH potentials for covalent geometry, nonbonded violations, gyration volume, HBDB (hydrogen-bonding database) potential, and RAMA (torsion angle database) were used in Xplor-NIH refinement. The final ensemble contains 20 structures with the lowest target function from 80 independent rounds.

Structure Validation and Analysis. Structures were visualized in MOLMOL (39) and PYMOL (www.pymol.org). Coordinates for PC2-EF and structural constraints have been deposited (PDB accession code: 2KQ6), and evaluated using PSVS ver. 1.3, with structure quality evaluators ProCheck, Prosall, and MolProbity (17).

ACKNOWLEDGMENTS. Syrus Meshack, Brenda DeGray, Yiqiang Cai and Stefan Somlo are thanked. This work was supported by National Institutes of Health (NIH) Grants P50 DK057328 (pilot to T.J.B., project to B.E.E.), DK061747 (to B.E.E.), CA108992 (to M.E.H.), CA009085 (training grant to E.T.P.), and a grant from the Polycystic Kidney Disease Foundation (B.E.E.). NMR structure determination was performed using the Yale University Biomedical High Performance Computing Center and NIH Grant RR19895, which funded the instrumentation.

1. Wu G, et al. (1998) Somatic inactivation of Pkd2 results in polycystic kidney disease. *Cell* 93(2):177–188.
2. Torres VE, Harris PC (2009) Autosomal dominant polycystic kidney disease: The last 3 years. *Kidney Int* 76(2):149–168.
3. Nauli SM, et al. (2003) Polycystins 1 and 2 mediate mechanosensation in the primary cilium of kidney cells. *Nat Genet* 33(2):129–137.
4. Koulen P, et al. (2002) Polycystin-2 is an intracellular calcium release channel. *Nat Cell Biol* 4(3):191–197.
5. Qian F, et al. (1997) PKD1 interacts with PKD2 through a probable coiled-coil domain. *Nat Genet* 16(2):179–183.
6. Casuscelli J, et al. (2009) Analysis of the cytoplasmic interaction between Polycystin-1 and Polycystin-2. *Am J Physiol-Renal* 297(5):1310–1315.
7. Celic A, et al. (2008) Domain mapping of the polycystin-2 C-terminal tail using de novo molecular modeling and biophysical analysis. *J Biol Chem* 283(42):28305–12.
8. Yu Y, et al. (2009) Structural and molecular basis of the assembly of the TRPP2/PKD1 complex. *Proc Natl Acad Sci USA* 106(28):11558–11563.
9. Kubota T, et al. (2009) New mutation of the Na channel in the severe form of potassium-aggravated myotonia. *Muscle Nerve* 39(5):666–673.
10. Xiao Q, et al. (2008) Regulation of bestrophin Cl channels by calcium: Role of the C terminus. *J Gen Physiol* 132(6):681–692.
11. Braun AP, Sy L (2001) Contribution of potential EF-hand motifs to the calcium-dependent gating of a mouse brain large conductance, calcium-sensitive K(+) channel. *J Physiol* 533(Pt 3):681–695.
12. Li Q, et al. (2002) The calcium-binding EF-hand in polycystin-L is not a domain for channel activation and ensuing inactivation. *FEBS Lett* 516(1–3):270–278.
13. Cantiello HF (2004) Regulation of calcium signaling by polycystin-2. *Am J Physiol-Renal* 286(6):F1012–1029.
14. Cai Y, et al. (2004) Calcium dependence of polycystin-2 channel activity is modulated by phosphorylation at Ser812. *J Biol Chem* 279(19):19987–19995.
15. Herrmann T, Guntert P, Wuthrich K (2002) Protein NMR structure determination with automated NOE assignment using the new software CANDID and the torsion angle dynamics algorithm DYANA. *J Mol Biol* 319(1):209–227.
16. Schwieters CD, et al. (2003) The Xplor-NIH NMR molecular structure determination package. *J Magn Reson* 160(1):65–73.
17. Bhattacharya A, Tejero R, Montelione GT (2007) Evaluating protein structures determined by structural genomics consortia. *Proteins* 66(4):778–795.
18. Nelson MR, Chazin WJ (1998) An interaction-based analysis of calcium-induced conformational changes in Ca^{2+} sensor proteins. *Protein Sci* 7(2):270–282.
19. Gifford JL, Walsh MP, Vogel HJ (2007) Structures and metal-ion-binding properties of the Ca^{2+}-binding helix-loop-helix EF-hand motifs. *Biochem J* 405(2):199–221.
20. Holm L, Sander C (1995) Dali: A network tool for protein structure comparison. *Trends Biochem Sci* 20(11):478–480.
21. Thompson JD, Higgins DG, Gibson TJ (1994) CLUSTAL W: Improving the sensitivity of progressive multiple sequence alignment through sequence weighting, position-specific gap penalties and weight matrix choice. *Nucleic Acids Res* 22(22):4673–4680.
22. Neill AT, Moy GW, Vacquier VD (2004) Polycystin-2 associates with the polycystin-1 homolog, suREJ3, and localizes to the acrosomal region of sea urchin spermatozoa. *Mol Reprod Dev* 67(4):472–477.
23. Otterbein LR, et al. (2002) Crystal structures of S100A6 in the Ca^{2+}-free and Ca^{2+}-bound states: The calcium sensor mechanism of S100 proteins revealed at atomic resolution. *Structure* 10(4):557–567.
24. Liepinsh E, Otting G, Wuthrich K (1992) NMR spectroscopy of hydroxyl protons in aqueous solutions of peptides and proteins. *J Biomol NMR* 2(5):447–465.
25. Biekofsky RR, et al. (1998) Ca^{2+} coordination to backbone carbonyl oxygen atoms in calmodulin and other EF-hand proteins: 15N chemical shifts as probes for monitoring individual-site Ca^{2+} coordination. *Biochemistry* 37(20):7617–7629.
26. Keeler C, Dannies PS, Hodsdon ME (2003) The tertiary structure and backbone dynamics of human prolactin. *J Mol Biol* 328(5):1105–1121.
27. Kneller JM, Lu M, Bracken C (2002) An effective method for the discrimination of motional anisotropy and chemical exchange. *J Am Chem Soc* 124(9):1852–1853.
28. Landau M, et al. (2005) ConSurf 2005: the projection of evolutionary conservation scores of residues on protein structures. *Nucleic Acids Res* 33(Web Server issue): W299–302.
29. Grishaev A, Bax A (2005) Weak alignment NMR: A hawk-eyed view of biomolecular structure. *Curr Opin Struc Biol* 15(5):563–570.
30. Schumann F, et al. (2009) Ca^{2+}-dependent conformational changes in a C-terminal cytosolic domain of polycystin-2. *J Biol Chem* 284(36):24372–24383.
31. Hooft RWW, Vriend G, Sander C, Abola EE (1996) Errors in protein structures. *Nature* 381:272.
32. Jaroszewski L, Pawlowski K, Godzik A (1998) Multiple model approach: Exploring the limits of comparative modeling. *J Mol Model* 4:294–309.
33. Berridge MJ (2006) Calcium microdomains: Organization and function. *Cell Calcium* 40(5–6):405–412.
34. Cai Y, et al. (1999) Identification and characterization of polycystin-2, the PKD2 gene product. *J Biol Chem* 274(40):28557–28565.
35. Ehrlich BE (1995) Functional properties of intracellular calcium-release channels. *Curr Opin Neurobiol* 5(3):304–309.
36. Ferrell JE, Jr (2009) Q&A: Cooperativity. *J Biol* 8(6):53.
37. Bezprozvanny I, Watras J, Ehrlich BE (1991) Bell-shaped calcium-response curves of Ins(1,4,5)P3- and calcium-gated channels from endoplasmic reticulum of cerebellum. *Nature* 351(6329):751–754.
38. Palmer AG (1997) Probing molecular motion by NMR. *Curr Opin Struc Biol* 7(5): 732–737.
39. Koradi R, Billeter M, Wuthrich K (1996) MOLMOL: a program for display and analysis of macromolecular structures. *J Mol Graphics* 14(1):51–55 29–32.
40. Zweckstetter M, Bax A (2000) Prediction of sterically induced alignment in a dilute liquid crystalline phase: Aid to protein structure determination by NMR. *J Am Chem Soc* 122(15):3791–3792.